



**HAL**  
open science

# The water vapor foreign continuum in the 8100-8500 cm<sup>-1</sup> spectral range

A.O. Koroleva, S. Kassi, D. Mondelain, A. Campargue

► **To cite this version:**

A.O. Koroleva, S. Kassi, D. Mondelain, A. Campargue. The water vapor foreign continuum in the 8100-8500 cm<sup>-1</sup> spectral range. *Journal of Quantitative Spectroscopy and Radiative Transfer*, 2023, 296, pp.108432. 10.1016/j.jqsrt.2022.108432 . hal-04221922

**HAL Id: hal-04221922**

**<https://hal.science/hal-04221922>**

Submitted on 20 Oct 2023

**HAL** is a multi-disciplinary open access archive for the deposit and dissemination of scientific research documents, whether they are published or not. The documents may come from teaching and research institutions in France or abroad, or from public or private research centers.

L'archive ouverte pluridisciplinaire **HAL**, est destinée au dépôt et à la diffusion de documents scientifiques de niveau recherche, publiés ou non, émanant des établissements d'enseignement et de recherche français ou étrangers, des laboratoires publics ou privés.

1 The water vapor foreign continuum  
2 in the 8100 - 8500 cm<sup>-1</sup> spectral range  
3  
4

5 A.O. Koroleva <sup>1,2</sup>, S. Kassi <sup>1</sup>, D. Mondelain <sup>1</sup>, A. Campargue <sup>1</sup>  
6

7 <sup>1</sup> *Univ. Grenoble Alpes, CNRS, LIPhy, Grenoble, France*  
8

9 <sup>2</sup> *Institute of Applied Physics of RAS, Nizhniy Novgorod, Russia*  
10  
11  
12  
13  
14  
15  
16  
17  
18  
19  
20  
21  
22  
23  
24  
25  
26  
27  
28  
29  
30  
31  
32  
33  
34  
35  
36  
37  
38  
39

40 *\*Corresponding author: Alain Campargue (alain.campargue@univ-grenoble-alpes.fr)*  
41  
42  
43  
44

45 **Key words**

46 Water vapor; foreign continuum; MT\_CKD model; CRDS; transparency window; atmosphere  
47

## Abstract

48  
49  
50  
51  
52  
53  
54  
55  
56  
57  
58  
59  
60  
61  
62  
63  
64

In the Earth's atmosphere, the foreign absorption continuum of water vapor is due to the interaction of water molecules with other atmospheric gases (mostly  $N_2$  and  $O_2$ ). Following our study of the self-continuum in the high energy edge of the 1.25  $\mu m$  transparency window (Korovela et al, J. Quant. Spectrosc. Radiat. Transfer 286 (2022) 108206), we report here the first room temperature measurements of water vapor foreign continuum in the same spectral region. Foreign continuum cross-sections,  $C_F$ , are derived at several selected spectral points between 8120 and 8500  $cm^{-1}$  for humidified nitrogen, humidified oxygen and humidified air (10000 ppm of  $H_2O$ ). The absorption signal is measured by cavity ring-down spectroscopy (CRDS) using pressure ramps up to 750 Torr. While the measured total continuum absorption follows nicely the expected quadratic dependence *versus* the total pressure, the uncertainty on the retrieved weak foreign continuum is strongly affected by other contributions which have to be subtracted from the measured absorption (far wings of the resonance lines,  $O_2$  collision induced absorption, self-continuum, Rayleigh scattering). The obtained  $H_2O$ -air and  $H_2O$ - $N_2$   $C_F$  cross-section values are found to be comparable while the  $H_2O$ - $O_2$   $C_F$  value appears to be significantly smaller. Overall, the retrieved  $C_F$  values for  $H_2O$ -air mixture validate the MT\_CKD model in the considered region.

65           **1.       Introduction**

66           The absorption of light by water vapor includes two main contributions: the well-known narrow  
67 rovibrational absorption lines (or resonance spectrum) and a broad-band contribution with weak  
68 frequency dependence, the continuum. In the Earth's atmosphere, the continuum includes the self-  
69 continuum and the foreign continuum related to water molecules in interaction with one another or  
70 with other atmospheric species (mostly N<sub>2</sub> and O<sub>2</sub>), respectively. As a result, the self-continuum varies  
71 as the square of the water vapor partial pressure,  $P_{H_2O}$ , while the foreign continuum is proportional to  
72  $P_{H_2O}P_F$  where  $P_F$  is the foreign gas pressure (dry air here) The water vapor absorption coefficient is  
73 thus expressed as:

$$\begin{aligned} \alpha_W(\nu, T) &= \alpha_{WML} + \alpha_{WCS} + \alpha_{WCF} \\ &= \alpha_{WML} + \frac{1}{kT} C_S(\nu, T) P_{H_2O}^2 + \frac{1}{kT} C_F(\nu, T) P_{H_2O} P_F \end{aligned} \quad (1)$$

74           where  $\alpha_{WML}$ ,  $\alpha_{WCS}$  and  $\alpha_{WCF}$  are the contributions due to resonant lines (WML), the water vapor  
75 self-continuum (WCS) and the foreign continuum (WCF), respectively.  $k$  is the Boltzmann constant,  
76  $P_{H_2O}$  and  $P_F$  are the water vapor and foreign gas partial pressures, respectively (thus  $P = P_{H_2O} + P_F$   
77 where  $P$  is the total pressure).  $C_S$  and  $C_F$  are the self- and foreign continuum cross-sections expressed  
78 in cm<sup>2</sup>molecule<sup>-1</sup>atm<sup>-1</sup>.  
79

80           Depending on the atmospheric conditions, the foreign continuum contribution to the absorption  
81 by water vapor can be of the same order as the self-continuum contribution which makes the  
82 characterization of both necessary. The semi-empirical MT\_CKD (Mlawer–Tobin–Clough–Kneizys–  
83 Davies) model [1,2,3] is the standard model implemented in climate and weather prediction models to  
84 account for the water continuum. In the windows between absorption bands, this model is mostly a  
85 far-wing line shape model with parameters empirically adjusted according to laboratory or  
86 atmospheric data at disposal, mostly in the infrared (*e.g.* [3-5]). In near-infrared windows, the original  
87 MT\_CKD cross-sections (*i.e.* MT\_CKD\_1.0 through \_3.0) thus resulted from long-range extrapolation  
88 which had to be validated.

89           Since 2013, we are involved in a long-term experimental project aiming to characterize the  
90 water vapor continuum mostly in the near-infrared windows where previous data were very scarce and  
91 reported with large uncertainties. Due to the weakness of the continuum signal, the measurements are  
92 performed using cavity enhanced absorption spectroscopy techniques (mostly cavity ring down  
93 spectroscopy - CRDS- but also optical feedback cavity enhanced absorption spectroscopy - OFCEAS)  
94 [7-17]. The cross-section derived at specific spectral point values are systematically used for  
95 validation tests of the current version of the MT\_CKD model. Although a number of significant  
96 deviations were evidenced (*e.g.* the MT\_CKD self-continuum in its 3.0 version was underestimated by  
97 a factor 5 to 10 near the centre of the 2.3 μm window [11-13, 16]), the measurements roughly  
98 validated the MT\_CKD values up to 8000 cm<sup>-1</sup> [17]. Considering the long-range spectral extrapolation  
99 of this semi-empirical model, this achievement deserves to be underlined. The most recent versions of

100 the MT\_CKD self-continuum (from V3.2) were refined according to our CRDS and OFCEAS  
101 experimental cross-sections in the 4.0, 2.1, 1.6 and 1.25  $\mu\text{m}$  windows [3].

102 As concerns the foreign continuum absorption, experimental data are scarcer [18], in particular  
103 at room temperature. In-band continuum measurements were reported in the 3500–4000  $\text{cm}^{-1}$  spectral  
104 range by direct absorption spectroscopy [6], between 1300 and 7500  $\text{cm}^{-1}$  by Fourier transform  
105 spectroscopy (FTS) [19] and in the 0.94  $\mu\text{m}$  absorption band by CRDS [20]. Of interest for the present  
106 investigation in the 1.25  $\mu\text{m}$  transparency window are the high temperature (350-430 K) foreign  
107 continuum FTS measurements by the CAVIAR consortium (Continuum Absorption at Visible and  
108 Infrared wavelengths and its Atmospheric Relevance) over the wide 1.1 - 5.0  $\mu\text{m}$  spectral range thus  
109 including the 1.25  $\mu\text{m}$  window of interest [21]. The comparison of our present room temperature  
110 measurements to the CAVIAR high temperature measurements might give insights on the temperature  
111 dependence of the foreign-continuum absorption which is known to be weak, much weaker than that  
112 of the self-continuum; the latter is known to decrease sharply with temperature.

113 In the transparency windows, measurements of the water foreign continuum are limited, in  
114 particular at room temperature, and spectrally dispersed. Cormier et al. [22] and Baranov&Lafferty  
115 [23] reported measurements in the 10  $\mu\text{m}$  window by CRDS and FTS, respectively. Water foreign  
116 continuum was determined in the 4.0  $\mu\text{m}$  window by FTS [23-25], in the 2.1 and 1.6  $\mu\text{m}$  windows by  
117 CRDS [9,14,15] and near 14400  $\text{cm}^{-1}$  by photoacoustic spectroscopy [26]. On the basis Refs. [9,22],  
118 the MT\_CKD foreign continuum has been significantly increased starting with version 2.8 [3].

119 To the best of our knowledge, no attempts were previously undertaken to measure the foreign  
120 continuum in the 1.25  $\mu\text{m}$  window at room temperature. Indeed, as described below the measurements  
121 are particularly demanding in this region due to the weak absorption signal to be measured and to the  
122 fact that the foreign contribution represents only a generally small fraction of the total measured  
123 absorption. In this situation, the derived foreign cross-section values are directly impacted by the  
124 evaluation of the other contributions (resonance lines broadened by  $\text{N}_2$ ,  $\text{O}_2$  or dry air,  $\text{O}_2$  collision  
125 induced absorption band near 1.27  $\mu\text{m}$ , self-continuum absorption, Rayleigh scattering) which have to  
126 be subtracted from the measured CRDS absorption coefficient. In order to help disentangling the  
127 different contributions, different series of measurements were performed using as foreign gas, pure  $\text{N}_2$ ,  
128 pure  $\text{O}_2$  and dry air. These three sets of derived  $C_F$  values will allow to test their self-consistency and  
129 discuss their uncertainties.

130 The remaining part of this paper is organized as follows: the data analysis is detailed in section  
131 3 after the description of the data acquisition in the next experimental section. In section 4, we discuss  
132 the consistency of our results and compare them to the MT\_CKD model [2,3] and to CAVIAR high  
133 temperature data [21].

## 134 **2. Experimental**

135 Water foreign continuum absorption measurements were performed by CRDS for a series of  
136 spectral points of the high energy edge of the 1.25  $\mu\text{m}$  window (8105 - 8480  $\text{cm}^{-1}$ ). The data

137 acquisition was performed at fixed frequency during pressure ramps of humidified gas (air, nitrogen  
138 and oxygen). The experimental approach is mostly the same as described in Ref. [17] for the self-  
139 continuum determination, except that the amplitude of the pressure ramps is much larger (up to 1 atm).  
140 The spectrometer uses an external cavity diode laser (ECDL, Toptica fiber-connected DL pro, 1200  
141 nm) as a light source. About 10% of the light intensity is sent to a wavelength meter (HighFinesse  
142 WSU7-IR, 5 MHz resolution, 20 MHz accuracy over 10 hours) which provides the laser frequency.  
143 The main part of the radiation is injected into the 1.4 m long CRDS cavity using a single mode fiber.  
144 The coincidence between the laser frequency and that of one mode of the CRDS cavity is achieved by  
145 modulating the rear mirror of the cavity mounted on a piezoelectric transducer (PZT), over about half  
146 the wavelength, over about half the wavelength, corresponding to the free spectral range of the cavity.  
147 At resonance, the cavity is filled with photons and then the injection of the laser light is interrupted by  
148 an acousto-optic modulator. An InGaAs PIN photodiode is used to measure the purely exponential  
149 decay time of photons leaking from the cavity. The absorption coefficient,  $\alpha(\nu)$ , is determined directly  
150 from fitted RD time,  $\tau$ :

$$\alpha(\nu) = \frac{1}{c\tau(\nu)} - \frac{1}{c\tau_0} \quad (1)$$

152 where  $c$  is the speed of light.  $\tau_0$  and  $\tau$  correspond to the ring down time of the cavity empty  
153 and filled with gas, respectively.

154 In the present experiments, Rayleigh scattering has a non-negligible contribution to the increase  
155 of the loss rate,  $\frac{1}{c\tau(\nu)}$ . (For convenience, “absorption coefficient” will be used in the following to name  
156 the increase of the loss rates due to both absorption and Rayleigh scattering).

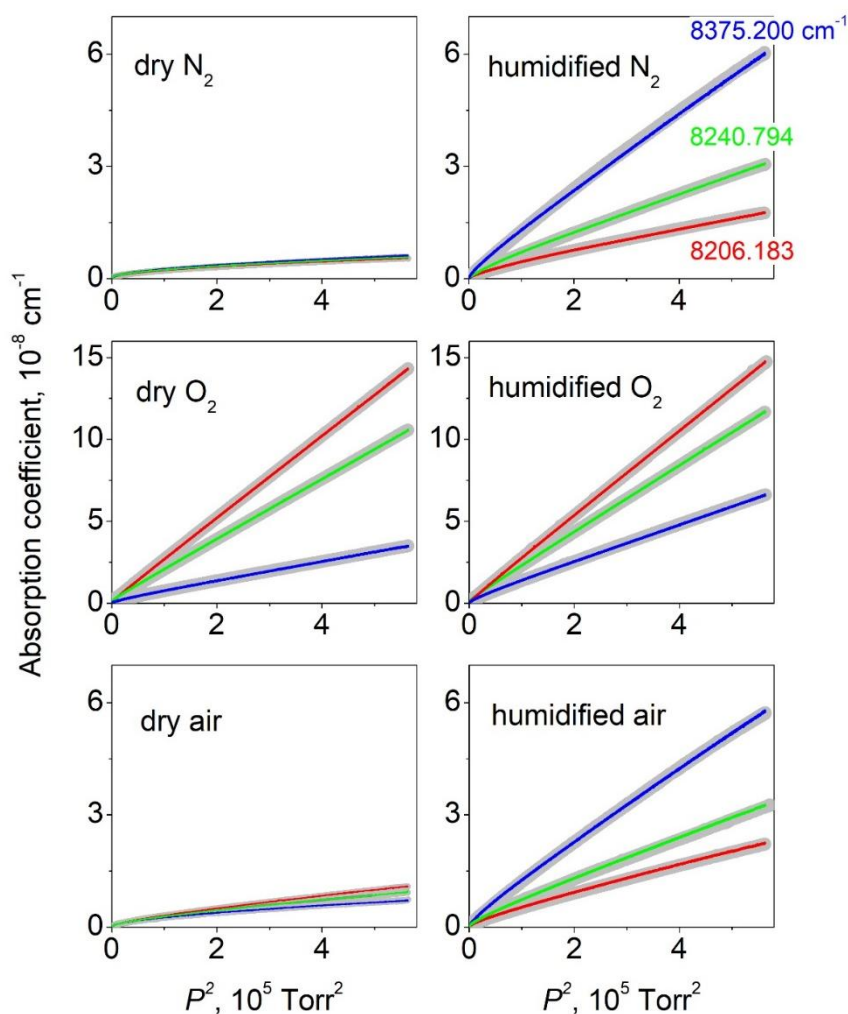
157 As in Ref. [17], the CRDS absorption signal is measured for series of pressure ramps at several  
158 fixed spectral points (from 5 to 8 depending on the gas mixture) selected in spectral microwindows  
159 minimizing the resonance line contribution (in fact, in the considered spectra region, the resonance  
160 line contribution is always large and remains the dominant contribution of the water-related absorption  
161 - see below). The chosen spectral points are part of the 29 spectral points used in Ref. [17] for the  
162 retrieval of the self-continuum absorption in the same region.

163 All the recordings are performed with a gas flow produced by a commercial humidity generator  
164 (from Omicron Technologies) (see Ref. [27] for a detailed description). The gas sample used for the  
165 recordings is a mixture of water vapor with 10,000 ppm molar fraction (*i.e.* 1%) in either synthetic air,  
166 N<sub>2</sub>, or O<sub>2</sub> (Alphagaz 2, 99,9995 % purity). Water vapor is produced from deionized liquid water in a  
167 temperature-regulated membrane system and then mixed with the carrier gas. The pressure and the gas  
168 flow in the gas line are controlled by a pressure controller (Model IQP-700C from Bronkhorst) and a  
169 mass flow controller (Area model, FC-R7800 series from Hitachi Metals Ltd.), respectively. The water  
170 concentration of the humidified gas is controlled by using the dew point temperature measured directly  
171 by the remote head of a precision chilled mirror hygrometer (Model S8000 from Mitchell). A small

172 part of the generated gas flow (typ. few tens of sccm) is directed inside the cavity where the pressure is  
173 varied between 0 and 750 Torr during the pressure ramps.

174 Two pressure gauges (10 and 1000 Torr full scale, from MKS Instruments, 0.25% of reading  
175 accuracy) are used to monitor continuously the total pressure in the cavity. A temperature sensor (TSic  
176 501 from IST,  $\pm 0.1$  K accuracy) fixed on the external wall of the cavity and enveloped by thermal  
177 insulation foam measure the temperature during the recordings. The temperature remains in the  
178  $294 \pm 1$  K range during the whole measurement campaign.

179 The humidified gas recordings include three steps: (i) increasing pressure ramp with a typical  
180 speed of 1 Torr/s (*i.e.* total duration of about 12 minutes), (ii) checking that the water partial pressure  
181 in the cell is constant by repetitive scan of a water line during about 1 hour and, (iii) decreasing  
182 pressure ramp (about 12 minutes). In addition, just after or just before this recording sequence, an  
183 additional recording is performed with the corresponding dry gas sample for an increasing and a  
184 decreasing pressure ramp. The dry gas pressure ramps measurements are used as baselines to be  
185 subtracted from humidified gas signal (see below).



186

187 **Fig. 1.**

188 Variation of the absorption coefficient *versus* the squared total pressure,  $P$ , during pressure  
189 ramps up to 750 Torr for three spectral points of the 1.25  $\mu\text{m}$  window (8206.183, 8240.794 and

190 8375.200  $\text{cm}^{-1}$  - red, green and blue curves, respectively). For each spectral point, measurements were  
191 performed during increasing and decreasing pressure ramps (grey and colored lines, respectively) for  
192 dry and humidified gas samples of synthetic air,  $\text{N}_2$  and  $\text{O}_2$  (left and right panels, respectively).



193 The variation of the absorption signal during increasing and decreasing pressure ramps with dry  
 194 and humidified samples are compared on **Fig. 1** for three spectral points. This figure deserves several  
 195 comments: (i) a nearly perfect superposition is observed for increasing and decreasing pressure  
 196 measurements, illustrating the stability of the experimental setup and allowing to use the averaged data  
 197 for further analysis, (ii) in the case of the O<sub>2</sub> measurements, the absorption signal is much larger than  
 198 for air and N<sub>2</sub> (note the different scales used in **Fig. 1**) as a result of the impact of the broad collision-  
 199 induced absorption (CIA) of the  $a^1\Delta_g - X^3\Sigma_g^-(0-0)$  band centered near 7900 cm<sup>-1</sup> [28]. This CIA  
 200 contribution is smaller at high energy which makes the absorption at 8375.200 cm<sup>-1</sup> smaller than those  
 201 at 8206.183 and 8240.794 cm<sup>-1</sup> in the case of O<sub>2</sub> while it is the opposite in the case of air and N<sub>2</sub>.

### 202 3. Cross-section retrieval

203 On the left panels of **Fig. 2**, the pressure ramps with humidified and dry gas are superimposed  
 204 for the 8240.794 cm<sup>-1</sup> spectral point. The water-related absorption presented on the right panels is  
 205 obtained by difference. It is important to mention, that the subtraction applies to absorption  
 206 coefficients corresponding to the same dry gas pressure and not to the same total pressure value. In  
 207 other words, the water-related absorption measured at a total pressure of  $P = P_{H_2O} + P_F$  was  
 208 decreased by the dry gas absorption at  $P_F$ . Ignoring the 1% difference between  $P$  and  $P_F$  in the  
 209 humidified gas sample would lead to negative water-related absorption in the case of humidified  
 210 oxygen as 1% of the O<sub>2</sub> CIA is larger than the O<sub>2</sub> foreign continuum absorption of water vapor. This  
 211 small contribution of the foreign continuum absorption to the measured absorption makes the accurate  
 212 retrieval of the water foreign continuum absorption particularly challenging in the region.

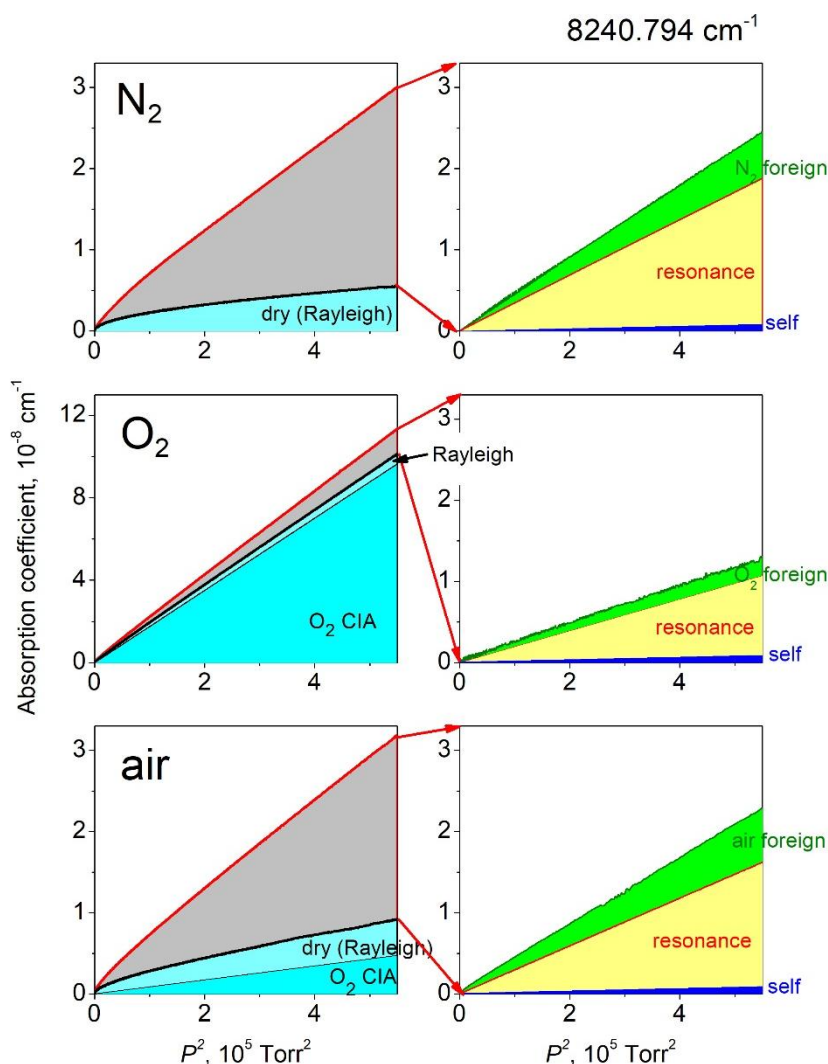
213 Let us first consider the dry gas recordings.

214 Rayleigh scattering is responsible of the variation of the loss rate during the dry N<sub>2</sub> pressure  
 215 ramps. Rayleigh scattering being proportional to pressure, it leads to a clear curvature for low pressure  
 216 values when plotted *versus* pressure squared both for dry and humidified N<sub>2</sub> (**Fig. 1** upper panels). As  
 217 Rayleigh scattering is mostly identical in the dry and humidified N<sub>2</sub> samples, the curvature nicely  
 218 vanishes in the water-related contribution obtained by difference and a nearly perfect quadratic  
 219 dependence *versus* the total pressure is achieved (**Fig. 2** right upper panel). Indeed, following **Eq. 1**,  
 220 the three contributions to the water-related absorption,  $\alpha_W(\nu, T)$ , have a pressure squared dependence  
 221 (the foreign contribution, proportional to  $P_{H_2O}P_F$  leads to a  $P^2$  dependence as the mixing ratio of water  
 222 in the dry gas is fixed to 1%).

223 Rayleigh scattering contribution of N<sub>2</sub> can be calculated from the refractive index coefficients  
 224 given in Ref. [29]. The measured losses induced by dry N<sub>2</sub> in our recordings are found about 50%  
 225 larger than expected from calculations. As a check of the calculated values obtained from Ref. [29],  
 226 we evaluated experimentally the refractive index from the variation of the frequency of the CRDS  
 227 cavity modes during an increasing pressure ramp of dry N<sub>2</sub> up to 1 atm. 643 modes were counted to  
 228 scroll during the filling and the evacuating of the cell at a fixed frequency of 8240.794 cm<sup>-1</sup>. It leads to

229 a refractive index of 1.000279 in perfect agreement with that used in Ref. [29]. The difference between  
 230 our observations and the calculated Rayleigh scattering losses could be related to mechanical changes  
 231 in the alignment of the CRDS cell induced by the change of pressure. This effect is believed to have  
 232 no impact on the retrieval of the water-related continuum absorption as, being reversible (as checked  
 233 by the consistency of the results obtained with increasing and decreasing pressure ramps), it is  
 234 cancelled in the subtraction of the humidified  $N_2$  and dry  $N_2$  signals.

235 In the case of oxygen (**Figs. 1 and 2**, middle panels), the absorption signal is largely dominated  
 236 by the CIA. The measured dry  $O_2$  absorption can be compared to calculated values obtained using the  
 237 CIA binary coefficients of Ref. [28] and the Rayleigh scattering coefficients of Ref. [29]. An excellent  
 238 agreement (better than 1%) is achieved.

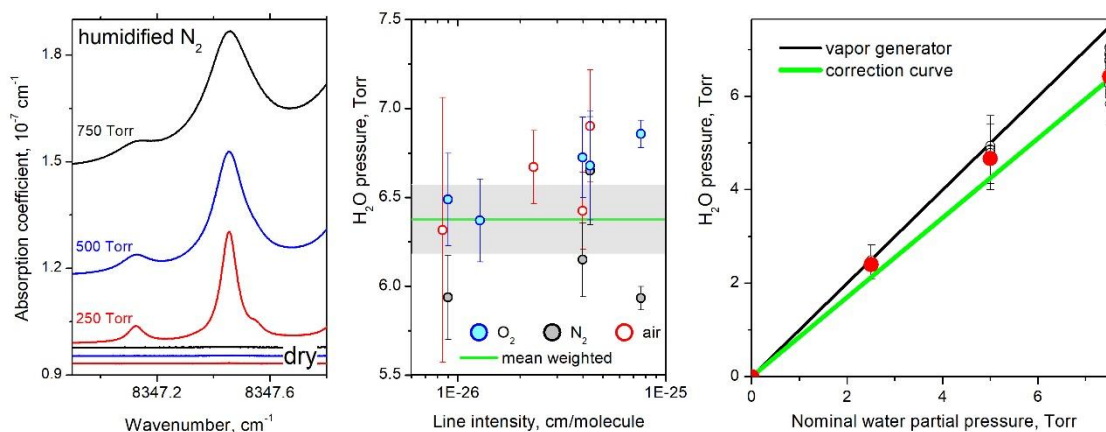


239  
 240 **Fig. 2.**  
 241 *Left panels:* Variation of the absorption coefficient *versus* the squared total pressure,  $P$ , for  
 242 humidified (red line) and dry (black line) gas samples during pressure ramps up to 750 Torr at the  
 243  $8240.794 \text{ cm}^{-1}$  spectral point. The dry gas “absorption” (cyan background) includes a Rayleigh  
 244 scattering contribution and a contribution of the CIA of the  $1.27 \mu\text{m}$  oxygen band (for  $O_2$  and air).  
 245 *Right panels:* The water-related absorption is obtained by difference of the humidified and dry  
 246 absorption and includes contributions of the water vapor self-continuum absorption (blue area), of the  
 247 resonance lines, (yellow area) and of the foreign continuum absorption (green area).

248 In the case of dry air, the calculated Rayleigh and CIA contributions, highlighted on the lower  
 249 panel of **Fig. 2**, have similar amplitude and our measurements are slightly larger than their predicted  
 250 sum. As for nitrogen, due to Rayleigh scattering losses, a nonlinear dependence on total pressure  
 251 squared is clearly observed (**Fig. 1** lower panels), but after subtraction of the dry part, the water-related  
 252 absorption pressure dependence becomes nicely linear *versus* the squared pressure (lower right panel  
 253 of **Fig. 2**).

254 Let us now considered the water-related absorption.

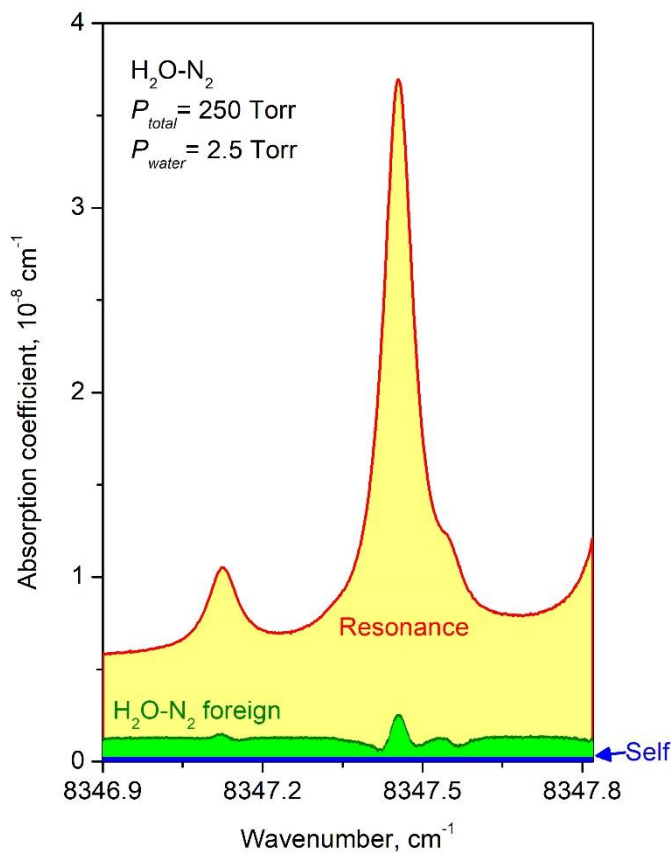
255 In the considered region corresponding to the high energy edge of the 1.25  $\mu\text{m}$  transparency  
 256 window, the resonance line contribution is the dominant part of the water-related absorption. We used  
 257 the same convention as adopted for the MT\_CKD model to simulate the resonance spectrum: line  
 258 profile was assumed to be of Voigt type and the line wings were truncated at  $\pm 25\text{ cm}^{-1}$  frequency  
 259 detuning from the line center, the underlying pedestal being considered as part of the continuum  
 260 absorption.



261  
 262 **Fig. 3.**  
 263 *Left panel:* CRDS spectra of 1% humidified  $\text{N}_2$  recorded at 250, 500 and 750 Torr total  
 264 pressures near  $8347\text{ cm}^{-1}$ . The three baselines at the bottom of the plot are the corresponding dry  $\text{N}_2$   
 265 spectra with level increasing linearly with pressure as a consequence of Rayleigh scattering losses,  
 266 *Middle panel:* Water vapor partial pressure values retrieved from a series of recordings of eight  
 267 lines of water broadened by  $\text{N}_2$ ,  $\text{O}_2$  or air at a total pressure of 750 Torr, *versus* their HITRAN line  
 268 intensities [30],  
 269 *Right panel:* Water vapor partial pressures retrieved from the line profile analysis *versus* the  
 270 nominal partial pressure (1% of the total pressure). The red dots correspond to the line at  $8347.46\text{ cm}^{-1}$   
 271 presented on the left panel. The pressure values presented corresponding to the nominal value of 7.5  
 272 Torr are those plotted on the middle panel. The linear fit of the experimental partial pressures *versus*  
 273 their nominal values gives a slope of 0.85 (green straight line). This factor was used to correct all the  
 274 water partial pressure values (see text).

275 A major issue of the current analysis is related to the knowledge of the real water vapor partial  
 276 pressure in the CRDS cell. Indeed, on the basis of spectra recorded over intervals corresponding to  
 277 mostly isolated water lines, it appeared that the simulation of the resonance line spectrum calculated  
 278 using the 10000 ppm relative concentration (corresponding to the set point of the humidity generator)

279 leads to an overestimation of the resonance line absorption. In other words, probably due to adsorption  
 280 effects, the real water pressure value in the cell is lower than its nominal value. In order to determine  
 281 its value, eight mostly isolated (broadened) water lines were selected and recorded for total pressure  
 282 values of humidified gas of 250, 500 and 750 Torr. **Fig. 3** shows an example of recorded line (left  
 283 panel), together with the different retrieved pressure values obtained from the eight lines broadened by  
 284 O<sub>2</sub>, N<sub>2</sub> or air *versus* their intensities (central panel) and the comparison with the nominal pressure  
 285 values (right panel). A weighted linear fit of the obtained  $P_{H_2O}$  values *versus* their nominal values (*i.e.*  
 286 1.00 % of the total pressure) was performed. The weight attached to each pressure value was fixed  
 287 according to its uncertainty resulting from the experimental noise, the fit uncertainty and the HITRAN  
 288 intensity uncertainty. As a result, the obtained partial pressure in the cell differs from its nominal value  
 289 in the gas by about 15% (green line **Fig. 3**, right panel). In the following analysis of the recorded  
 290 pressure ramps, this correction will be applied to all the (nominal) water vapor partial pressures. In  
 291 spite of the high signal-to-noise level of the recorded spectra and our careful analysis of about twenty  
 292 water line recordings, the large broadening of the line profile makes an accurate determination of the  
 293 line area difficult (due to baseline uncertainty). As a result, the uncertainty on the amplitude of the  
 294 pressure correction remains a potential source of uncertainty on the derived foreign cross-section  
 295 values (see below).



296  
 297 **Fig. 4.**

298 The different contributions to the water-related absorption in humidified (1%) N<sub>2</sub> at a total  
 299 pressure of 250 Torr, near 8347 cm<sup>-1</sup>: self-continuum (blue), H<sub>2</sub>O-N<sub>2</sub> foreign continuum (green) and  
 300 resonance line contribution (yellow).

301  
 302 As mentioned above, the water resonance line contribution was simulated as a sum of Voigt line  
 303 profiles with the standard  $\pm 25$  cm<sup>-1</sup> wing cut-off. Line intensities, self- and air-broadening coefficients  
 304 were taken from the HITRAN2020 database [30]. N<sub>2</sub>- and O<sub>2</sub>-broadening coefficients of water lines  
 305 are not provided in the HITRAN lists. The water line broadening parameters by N<sub>2</sub> ( $\gamma_{N_2}$ ) were  
 306 calculated in [31] in the frame of MCRB formalism and the ‘‘HITRAN’’ list attached to this work as  
 307 supplementary material, including  $\gamma_{N_2}$ , was adopted. Oxygen-broadening coefficients of each water  
 308 line,  $\gamma_{O_2}$ , were calculated using the equation  $\gamma_{air} = 0.79\gamma_{N_2} + 0.21\gamma_{O_2}$ , using  $\gamma_{air}$ , and  $\gamma_{N_2}$  from  
 309 HITRAN2020 and Ref. [31], respectively.

310 The last contribution which has to be subtracted is the water self-continuum (see Eq. 1). It was  
 311 calculated using the self-continuum cross-section values derived by CRDS of pure water vapor [17].  
 312 The different contributions to the water-related absorption are separated on **Fig. 4** in a small spectral  
 313 interval around 8347 cm<sup>-1</sup>. After the subtraction of the resonance line contribution, significant  
 314 residuals are obtained near the line centres as a result of some inaccuracies of the line parameters used  
 315 to compute the resonance line spectrum. The foreign continuum absorption represents less than 20%  
 316 of the water-related absorption illustrating the difficulty of an accurate evaluation.

317 On the right panels of **Fig. 2**, the different contributions are presented during the pressure ramp  
 318 at 8240.794 cm<sup>-1</sup>. The self-continuum contribution is small (a few %) while the resonance line  
 319 contribution represents about 70% of the total absorption. This is a typical situation for all the  
 320 measurement points listed in **Table 1**: in spite of a careful selection of microwindows minimizing the  
 321 resonance line contribution, the latter represents most of the water-related absorption at all  
 322 measurement points. The relative contribution of the resonance line to the water-related absorption  
 323 (ranging between 61 and 83%) is given in **Table 1** for each spectral point.

324 **Table 1**  
 325 Foreign gas cross-sections of water vapor ( $C_F$ ) derived at nine spectral points between 8100 and  
 326 8500 cm<sup>-1</sup>.

Wavenumber, cm <sup>-1</sup>	$C_F$ 10 <sup>-27</sup> cm <sup>2</sup> molecule <sup>-1</sup> atm <sup>-1</sup>			Resonance absorption %			Uncertainty due to resonance spectrum 10 <sup>-27</sup> cm <sup>2</sup> molecule <sup>-1</sup> atm <sup>-1</sup>		
	N <sub>2</sub>	O <sub>2</sub>	air	N <sub>2</sub>	O <sub>2</sub>	air	N <sub>2</sub>	O <sub>2</sub>	air
8105.865	-	5.3(3)	-	-	49.6	-	-	2.1	-
8123.155	7.6(1.1)	0.3(2)	3.8(9)	68.6	82.6	77.0	2.3	3.8	4.4
8206.183	19(2)	7.7(8)	19.1(1.9)	63.1	67.2	61.3	4.1	6.3	7.6
8240.794	33(4)	10.1(1.9)	33.0(3.7)	69.8	77.7	67.6	8.8	14.2	16.9
8279.585	-	-	53.5(7.0)	-	-	72.4	-	-	34.3
8317.615	-	26.7(4.7)	-	-	76.1	-	-	32.3	-
8375.200	68.2(8.5)	25.9(5.1)	62.0(8.0)	71.4	78.0	71.8	14.3	33.8	32.3
8434.240	-	52.1(6.9)	-	-	68.8	-	-	40.2	-
8480.505	104(11)	33.3(6)	88.4(10.0)	66.5	74.2	67.8	12.9	37.5	42.0

327  
 328 *Notes*

329 Columns 2-4:  $C_F$  values for  $N_2$ ,  $O_2$  and air, respectively, with corresponding experimental  
330 uncertainty given between parenthesis. The uncertainty value is limited to the statistical fit uncertainty  
331 and water partial pressure uncertainty,

332 Columns 5-7: Corresponding fraction (in %) of the resonance absorption contribution to the  
333 water-related absorption,

334 Columns 8-10: Uncertainty related to the subtraction of the resonance absorption contribution  
335 evaluated on the basis of the errors on the HITRAN line parameters.

336  
337 The pressure dependence of the water-related absorption after subtraction of the self-continuum  
338 and resonance lines contributions is presented in **Fig. 5** for air,  $N_2$  and  $O_2$  pressure ramps at three  
339 measurement points. A good pressure squared dependence is achieved as expected from Eq. 1 (recall  
340 that  $P_{H_2O}$  and  $P$  are proportional). Note that the plotted ramps are in fact the superposition of the  
341 increasing and decreasing pressure ramp signals. The foreign continuum cross-sections listed in **Table**  
342 **1** were obtained from a linear fit of the pressure dependences using Eq. 1.

343

344

345

346

347

348

349

350

351

352

353

354

355

356 **Fig. 5.**

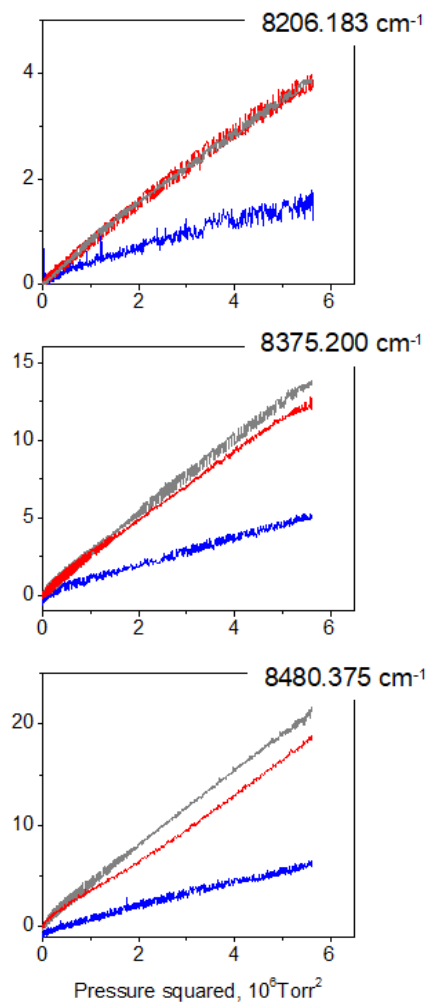
357 Variation of the absorption coefficient corresponding to  
358 the foreign gas contribution *versus* the squared total pressure,  
359  $P$ , during pressure ramps up to 750 Torr for three spectral  
360 points of the 1.25  $\mu m$  window (8206.183, 8375.200 and  
361 8480.375  $cm^{-1}$ ). Traces in grey, blue and red correspond to gas  
362 samples of humidified (10000 ppm)  $N_2$ ,  $O_2$  and synthetic air,  
363 respectively. Each curve corresponds to the measured  
364 absorption signal decreased by the dry gas contribution, the  
365 resonance gas contribution and the water self-continuum and is  
366 the superposition of the increasing and decreasing pressure  
367 ramps.

368

369

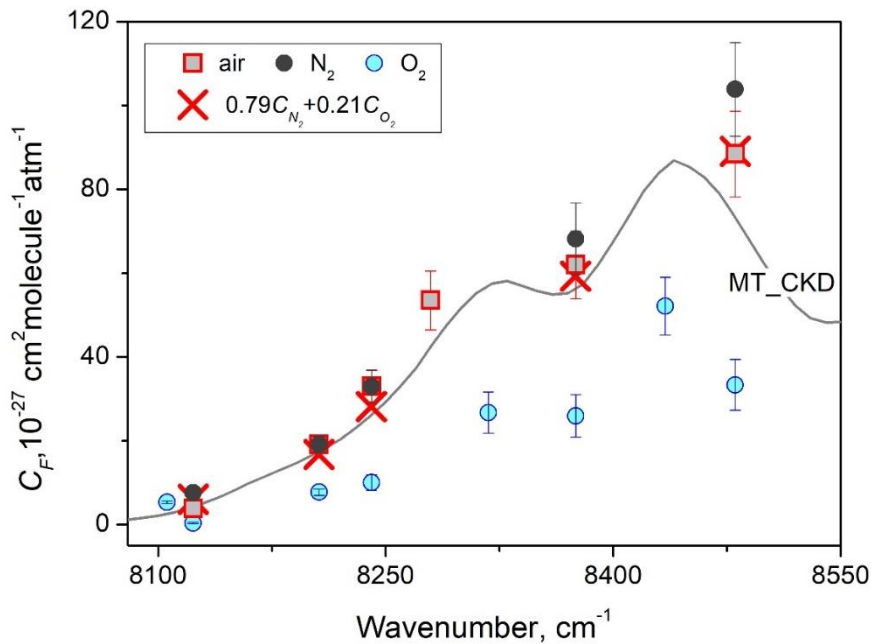
#### 4. Discussion and concluding remarks

370 **Fig. 6** shows an overview of the retrieved foreign cross-sections. The plotted error bars are  
371 limited to the experimental uncertainties on the (corrected) value of the water partial pressure (about  
372 3%), and on the linear coefficient of the pressure ramp fit (on the order of 1 % for  $N_2$  and  $O_2$  and up to



373 15% for air). It should be pointed that the above 15 % correction of the partial pressure of water in the  
 374 cell has an important impact on the obtained  $C_F$  values. In absence of correction,  $C_{N_2}$  and  $C_{air}$  values  
 375 would have been smaller by a factor 2-3 while the  $C_{O_2}$  cross-sections would have been decreased to a  
 376 level too weak to be evaluated.

377 As in the retrieval of the water self-continuum cross-sections in the same region [17], an  
 378 additional important error source should be considered. It is related to the evaluation of the resonance  
 379 line contribution which represents 60-80% of the water-related absorption and has thus a direct impact  
 380 on the retrieved  $C_F$  values. In other words, the obtained  $C_F$  values cannot be dissociated from the  
 381 resonance line databases we used for their retrieval. Based on the error codes attached to the HITRAN  
 382 line parameters [30], we evaluated the uncertainty on the resonance line contribution. The obtained  
 383 error bars included in **Table 1** are sometimes comparable to our absolute  $C_F$  values. This problematic  
 384 situation may indicate that our obtained  $C_F$  values should be used with much caution or/and that the  
 385 HITRAN error bars are overestimated. There is some indication that HITRAN uncertainties on the  
 386 broadening parameters are indeed overestimated: in the case of  $N_2$ , the uncertainties on the resonance  
 387 line contribution included in **Table 1** were obtained from the ‘‘HITRAN’’ list produced by Vispoel et  
 388 al. [31] (where error values are attached to each  $N_2$ -broadening coefficient instead of error codes given  
 389 in HITRAN for air-broadening coefficients). As a result, the obtained resonance line uncertainties are  
 390 2-3 times smaller for  $N_2$  than for air (see **Table 1**).



391 **Fig. 6.**  
 392 Overview of the foreign continuum cross-sections,  $C_F$ , retrieved for  $N_2$  (black dots),  $O_2$  (blue  
 393 dots) and dry air (red squares) between 8100 and 8500  $cm^{-1}$  and comparison to the values provided for  
 394 air by the MT\_CKD\_V3.5. The red crosses correspond to the calculated values of  $C_{air}$  obtained from  
 395  $C_{air}=0.79C_{N_2}+0.21C_{O_2}$ . The plotted error bars are those given in Columns 2-4 of Table 1 and are  
 396 limited to the combined impact of the uncertainty on the water partial pressure (about 3%) and on the  
 397 linear coefficient of the pressure ramp fit (see Text).  
 398

399 In spite of the doubts on the estimation of the error bars, a number of observations give some  
400 confidence to our results:

401 (i) The overall consistency between the  $C_{N_2}$  and  $C_{air}$  values, determined independently, is very  
402 good, the  $C_{N_2}$  values being generally larger than  $C_{air}$  values,

403 (ii) Air foreign continuum cross-sections calculated as  $C_{air}=0.79C_{N_2}+0.21C_{O_2}$  (red crosses in  
404 **Fig. 6**) nicely agree with the direct experimental determinations of  $C_{air}$  (red squares) illustrating the  
405 self-consistency of three sets of measurements:  $C_{O_2}$  values being smaller than  $C_{N_2}$  and  $C_{air}$  values, the  
406 differences between  $C_{N_2}$  and  $C_{air}$  values are close to the calculated impact of the  $O_2$  contribution on  
407  $C_{air}$  values,

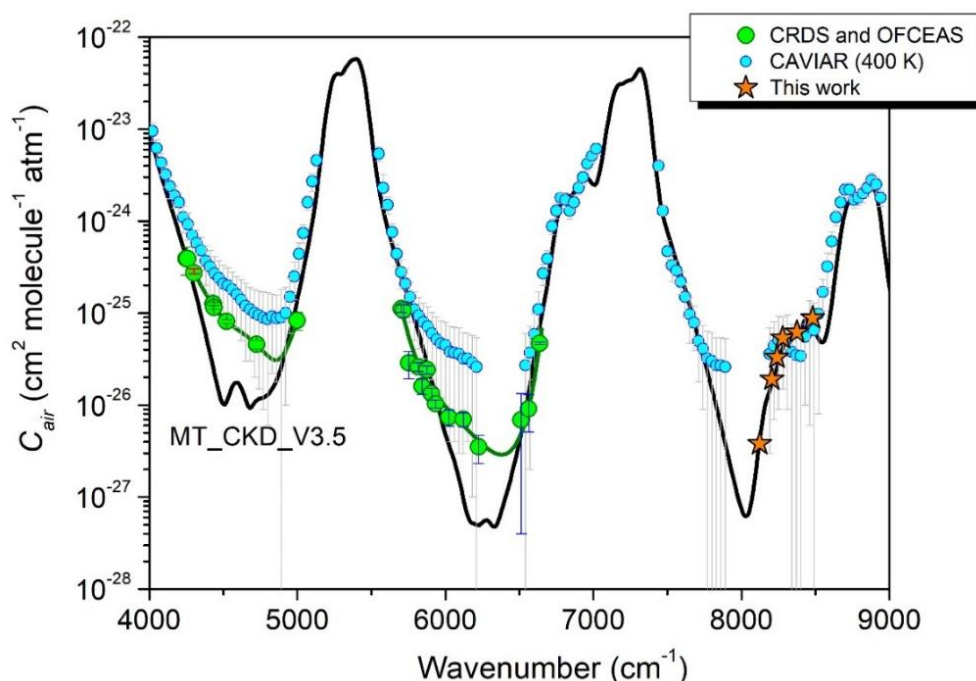
408 (iii) The comparison of experimental and calculated  $C_{air}$  values with the MT\_CKD model  
409 shows an overall good agreement. We also note that  $C_{O_2}$  frequency dependence is consistent with the  
410 two maxima of the MT\_CKD model.

411 From **Table 1** and **Fig. 6**, it appears that the foreign cross-sections are significantly smaller for  
412  $O_2$  than for  $N_2$ . In the literature, the dependence of the water foreign continuum upon the nature of the  
413 foreign gas has been rarely discussed. In several experimental studies using  $N_2$  as foreign gas, the  
414 obtained water- $N_2$  cross-sections are compared to the MT\_CKD model (thus for air) with the implicit  
415 assumption that water- $O_2$  and water- $N_2$  cross-sections are close. In fact, little is known on the water- $O_2$   
416 foreign continuum. To the best of our knowledge, the only previous study which reported water  
417 foreign cross-section for  $O_2$ ,  $N_2$  and air was performed in the far infrared (FIR) [32]. Although the  
418 strong resonance line contribution was a limiting factor of the analysis (as in the present study), the  
419 water- $O_2$  continuum in the rotational region ( $50-700\text{ cm}^{-1}$ ) was found largely smaller than the water- $N_2$   
420 and water-air continua (in fact,  $C_{O_2}$  appeared to be too weak to be experimentally determined *i.e.* more  
421 than five times smaller than,  $C_{N_2}$  and  $C_{air}$  – see Fig. 6 of Ref. [32]). Here, the measurement of the  
422 water- $O_2$  continuum is made even more challenging due to the overlapping with the CIA band of  $O_2$   
423 near  $1.27\text{ }\mu\text{m}$ . At the  $8240.794\text{ cm}^{-1}$  spectral point of **Fig. 2**, the water-related absorption represents  
424 about 10% of the measured absorption and the  $O_2$ -foreign itself no more than 1.6 % which obliges to  
425 some caution when considering the derived  $C_{O_2}$  values. Nevertheless, the obtained frequency  
426 dependence of  $C_{O_2}$  appears to be reasonable which gives some credit to the evidenced smaller  
427 amplitude of the water- $O_2$  continuum compared to the water- $N_2$  continuum. Although the oxygen  
428 concentration in air is only 21%, the resulting decrease of the water-air continuum compared to the  
429 water- $N_2$  continuum is consistent with the observations (see **Fig. 6**).

430 Note that in the frame of the far wings interpretation of the water foreign continuum, the water-  
431  $O_2$  and the water- $N_2$  continua are expected to scale according to the corresponding water broadening  
432 coefficients. Roughly, the broadening coefficients of water lines by  $O_2$  are on average 30% smaller  
433 than those by  $N_2$ . This factor appears to be not far from the scaling factor of the  $C_{O_2}$  and  $C_{N_2}$  cross-  
434 sections determined in the present work but disagrees with the FIR observations [32].



435 We have gathered in **Fig. 7**, the room temperature water-air foreign cross-sections derived in  
 436 this work and in our previous CRDS studies in the 2.3 and 1.6  $\mu\text{m}$  windows [9,14,15], and compared  
 437 them to the MT\_CKD\_V3.5 foreign continuum. A clear underestimation of the MT\_CKD model was  
 438 evidenced in the 2.3 and 1.6  $\mu\text{m}$  windows, which is not the case in the presently studied 1.25  $\mu\text{m}$   
 439 where the MT\_CKD model is validated. The foreign (air) cross-sections reported by the CAVIAR  
 440 consortium [21] have been superimposed on the plot. The CAVIAR measurements by FTS were  
 441 performed at 350, 372, 402 and 431 K (which allowed to increase the absorption signal by increasing  
 442 the water partial pressure to a few hundreds of mbar). In the 1.25  $\mu\text{m}$  window, the large ( $1\sigma$ ) error bars  
 443 of the CAVIAR measurements (on the order of 100%) do not allow a sound comparison. Nevertheless,  
 444 the order of magnitude of CAVIAR  $C_{air}$  values at 400 K is reasonable compared to our room  
 445 temperature measurements (let us recall that the temperature dependence of the foreign continuum is  
 446 known to be very weak).



447 **Fig. 7.**  
 448 Overview of the water foreign continuum cross-sections,  $C_{air}$  between 4000 and 9000  $\text{cm}^{-1}$   
 449 obtained in this work and found in the literature [9,14,15, 21], and comparison to the MT\_CKD\_V3.5  
 450 model. The CAVIAR experimental values [21] were obtained at 400 K while the other displayed  
 451 values correspond to the room temperature.  
 452

453  
 454 As a final conclusion, the first (challenging) measurements of the air-,  $\text{O}_2$ -, and  $\text{N}_2$ -water  
 455 continua at room temperature have been performed in the 1.25  $\mu\text{m}$  window for a series of pressure  
 456 ramps at fixed spectral points. The humidity rate was fixed to 1% and the measured total continuum  
 457 absorption were found to follow satisfactorily the expected quadratic dependence *versus* the total  
 458 pressure up to 1 atm. In spite of the sensitivity and stability of the used CRDS setup (illustrated by the  
 459 obtained pressure squared dependences), the accuracy of our final cross-section values is limited. As

460 the foreign continuum represents of small fraction of the measured absorption signal and as some of  
461 the other contributions (far wings of the resonance lines, O<sub>2</sub> collision induced absorption, self-  
462 continuum, Rayleigh scattering) are known with large uncertainties (*e.g.* resonance line absorption),  
463 we cannot claim a high accuracy on the reported cross-section values. In addition, the real humidity  
464 rate in the CRDS cell had to be estimated from a line profile analysis which led to a correction of 15%  
465 compared to its nominal value. Altogether, we roughly estimate as 50% the overall error bars on our  
466 cross-section values. The agreement with the MT\_CKD model, unexpectedly better than this error bar,  
467 might be coincidental. We thus conclude that in the 1.27 μm transparency window, the MT\_CKD  
468 model is validated within our uncertainties, which was not the case in the 2.3 and 1.6 μm windows,  
469 where an underestimation of the MT\_CKD values by up to a factor 10 were measured in the centers of  
470 the windows [9,14,15].

471 The question of the relative amplitude of the O<sub>2</sub>-, and N<sub>2</sub>-water continua deserves further  
472 investigation in more favorable spectral ranges. The 1.6 μm window is considered for dedicated study  
473 of this issue.

474

#### 475 **CRedit authorship contribution statement**

476 **A. O. Koroleva:** Investigation. **S. Kassi:** Investigation. **D. Mondelain:** Investigation. **A. Campargue:**  
477 Investigation.

478

#### 479 **Acknowledgements**

480 This project is supported by the French National Research Agency in the framework of the "In-  
481 vestissements d'avenir" program (ANR-15-IDEX-02) and by CNRS (France) in the frame of the  
482 International Research Project "SAMIA". We would like to thank Robert Gamache (University of  
483 Massachusetts Lowell) for valuable discussion about the water broadening coefficients by N<sub>2</sub> and O<sub>2</sub>.

- 485 1. Clough SA, Kneizys FX, Davies RW. Line shape and the water vapor continuum. *Atm Res*  
486 1989;23:229-241. doi:10.1016/0169-8095(89)90020-3
- 487 2. Mlawer EJ, Payne VH, Moncet J, Delamere JS, Alvarado MJ, Tobin DC. Development and  
488 recent evaluation of the MT\_CKD model of continuum absorption. *Phil Trans R Soc A*  
489 2012;370:2520–2556. doi:10.1098/rsta.2011.0295
- 490 3. [https://github.com/AER-RC/MT\\_CKD/](https://github.com/AER-RC/MT_CKD/)
- 491 4. Burch DE. Continuum absorption by H<sub>2</sub>O. Report AFGL-TR-81-0300, Air Force Geophys.  
492 Laboratory, Hanscom AFB, MA, 1982.
- 493 5. Burch DE, Alt RL. Continuum absorption by H<sub>2</sub>O in the 700 – 1200 cm<sup>-1</sup> and 2400 – 2800  
494 cm<sup>-1</sup> windows. Report AFGL-TR-84-0128, Air Force Geophys. Laboratory, Hanscom AFB,  
495 MA, 1984.
- 496 6. Burch DE. Absorption by H<sub>2</sub>O in narrow windows between 3000 and 4200 cm<sup>-1</sup>. Report  
497 AFGL-TR-85-0036, Air Force Geophys. Laboratory, Hanscom AFB, MA, 1985.
- 498 7. Mondelain D, Aradj A, Kassi S, Campargue A. The water vapor self-continuum by CRDS at  
499 room temperature in the 1.6 μm transparency window. *J Quant Spectrosc Radiat Transfer*  
500 2013;130:381–91. doi: 10.1016/j.jqsrt.2013.07.006.
- 501 8. Mondelain D, Manigand S, Manigand S, Kassi S, Campargue A. Temperature dependence of  
502 the water vapor self-continuum by cavity ring-down spectroscopy in the 1.6 μm transparency  
503 window. *J Geophys Res Atmos* 2014;119(9):2169–8996. doi: 10.1002/2013JD021319.
- 504 9. Mondelain D, Vasilchenko S, Čermák P, Kassi S, Campargue A. The self- and foreign-  
505 absorption continua of water vapor by cavity ring-down spectroscopy near 2.35 μm. *Phys*  
506 *Chem Chem Phys* 2015;17:17,762–17,770. doi: 10.1039/c5cp01238d
- 507 10. Ventrillard I, Romanini D, Mondelain D, Campargue A. Accurate measurements and  
508 temperature dependence of the water vapor self-continuum absorption in the 2.1 μm  
509 atmospheric window. *J Chem Phys* 2015;143:134304. doi: 10.1063/1.4931811]
- 510 11. Campargue A, Kassi S, Mondelain D, Vasilchenko S, Romanini D. Accurate laboratory  
511 determination of the near infrared water vapor self-continuum: A test of the MT\_CKD model.  
512 *J Geophys Res Atmos* 2016;121:13,180 – 13,203. doi:10.1002/2016JD025531
- 513 12. Richard L, Vasilchenko S, Mondelain D, Ventrillard I, Romanini D, Campargue A. Water  
514 vapour self-continuum absorption measurements in the 4.0 and 2.1 μm transparency windows.  
515 *J Quant Spectrosc Radiat Transf* 2017;201:171–179. doi: 10.1016/j.jqsrt.2017.06.037
- 516 13. Lechevallier L, Vasilchenko S, Grilli R, Mondelain D, Romanini D, Campargue A. The water  
517 vapour self-continuum absorption in the infrared atmospheric windows: new laser  
518 measurements near 3.3 and 2.0 μm. *Atmos Meas Tech* 2018;11:2159–2171. doi:10.5194/amt-  
519 11-2159-2018
- 520 14. Vasilchenko S, Campargue A, Kassi S, Mondelain D, The water vapour self- and foreign-  
521 continua in the 1.6 μm and 2.3 μm windows by CRDS at room temperature. *J Quant Spectrosc*  
522 *Radiat Transfer* 2019;227:230–238. doi: 10.1016/j.jqsrt.2019.02.01
- 523 15. Mondelain D, Vasilchenko S, Kassi S, Campargue A, The water vapor foreign-continuum in  
524 the 1.6 μm window by CRDS at room temperature. *J Quant Spectrosc Radiat Transfer*  
525 2020;246:106923. [doi.org/10.1016/j.jqsrt.2020.106923](https://doi.org/10.1016/j.jqsrt.2020.106923)
- 526 16. Fleurbaey H, Grilli R, Mondelain D, Campargue A. Measurements of the water vapor  
527 continuum absorption by OFCEAS at 3.50 μm and 2.32 μm. *J Quant Spectrosc Radiat Transf*  
528 2022;278:108004. doi.org/10.1016/j.jqsrt.2021.108004
- 529 17. Koroleva AO, Kassi S, Campargue A. The water vapor self-continuum absorption at room  
530 temperature in the 1.25 μm window. *J Quant Spectrosc Radiat Transf* 2022;286:108206.  
531 <https://doi.org/10.1016/j.jqsrt.2022.108206>
- 532 18. Hartmann J-M, Tran H, Armante R, Boulet C, Campargue A, Forget F, Gianfrani L, Gordon I,  
533 Guerlet S, Gustafsson M, Hodges JT, Kassi S, Lisak D, Thibault F, Toon GC. Recent  
534 advances in collisional effects on spectra of molecular gases and their practical consequences,  
535 *J Quant Spectrosc Radiat Transfer* 2018;213:178–227. doi: 10.1016/j.jqsrt.2018.03.016

- 536 19. Paynter D J, Ptashnik I V, Shine K P, Smith K M, McPheat R, Williams R G 2009 Laboratory  
537 measurements of the water vapour continuum in the 1200–8000  $\text{cm}^{-1}$  region between 293K  
538 and 351 K. *J Geophys Res* 114, D21301. doi:10.1029/2008JD011355
- 539 20. Reichert L, Andrés Hernández MD, Burrows JP, Tikhomirov AB, Firsov KM, Ptashnik IV.  
540 First CRDS-measurements of water vapour continuum in the 940 nm absorption band. *J Quant*  
541 *Spectrosc Radiat Transf* 2007;105:303–11. doi: 10.1016/j.jqsrt.2006.10.010.
- 542 21. Ptashnik IV, McPheat RA, Shine KP, Smith KM, Williams RG. Water vapour foreign-  
543 continuum absorption in near-infrared windows from laboratory measurements. *Phil Trans R*  
544 *Soc A* 2012;370: 2557–2577. doi:10.1098/rsta.2011.0218
- 545 22. Baranov YI. The continuum absorption in  $\text{H}_2\text{O}+\text{N}_2$  mixtures in the 2000–3250  $\text{cm}^{-1}$  spectral  
546 region at temperatures from 326 to 363 K. *J Quant Spectrosc Radiat Transfer* 2011;112:2281–  
547 2286. doi:10.1016/j.jqsrt.2011.06.005
- 548 23. Baranov YI, Buryak IA, Lokshantov SE, Lukyanchenko VA, Vigasin AA.  $\text{H}_2\text{O}-\text{N}_2$  collision-  
549 induced absorption band intensity in the region of the  $\text{N}_2$  fundamental: ab initio investigation  
550 of its temperature dependence and comparison with laboratory data. *Phil Trans R Soc A*  
551 2012;370:2691–2709. doi: 10.1098/rsta.2011.0189.
- 552 24. Baranov YI and Lafferty WJ. The water vapour self- and water-nitrogen continuum absorption  
553 in the 1000 and 2500  $\text{cm}^{-1}$  atmospheric windows. *Phil Trans R Soc A* 2012;370:2578–2589.  
554 doi: 10.1098/rsta.2011.0234
- 555 25. Cormier JG, Hodges JT, Drummond JR. Infrared water vapor continuum absorption at  
556 atmospheric temperatures. *J Chem Phys* 2005;122:114309. doi: 10.1063/1.1862623.
- 557 26. Tikhomirov AB, Ptashnik IV, Tikhomirov BA. Measurements of the continuum absorption  
558 coefficient of water vapour near 14400  $\text{cm}^{-1}$  (0.694  $\mu\text{m}$ ). *Opt Spectrosc* 2006;101:80.
- 559 27. Fleurbaey H, Campargue A, Carreira Mendès Da Silva Y, Grilli R, Kassi S, Mondelain D.  
560 Characterization of the  $\text{H}_2\text{O}+\text{CO}_2$  continuum within the infrared transparency windows. *J*  
561 *Quant Spectrosc Radiat Transf* 2022;282:108119. <https://doi.org/10.1016/j.jqsrt.2022.108119>
- 562 28. Mondelain D, Kassi S, Campargue A. Accurate Laboratory Measurement of the  $\text{O}_2$  Collision-  
563 Induced Absorption Band Near 1.27  $\mu\text{m}$ . *J Geophys Res Atmos* 2018;124(1),414 - 423.  
564 <https://doi.org/10.1029/2018JD029317>
- 565 29. Thalman R, Zarzana K, Tolbert MA, Volkamer R. Rayleigh scattering cross- section  
566 measurements of nitrogen, argon, oxygen and air. *J Quant Spectrosc Radiat Transf*  
567 2014;147:171–7. doi: 10.1016/j.jqsrt.2014.05.030
- 568 30. Gordon IE, Rothman LS, Hargreaves RJ, Hashemi R, Karlovets EV, Skinner FM, et al. The  
569 HITRAN2020 molecular spectroscopic database. *J Quant Spectrosc Radiat Transf*  
570 2022;277:107949. <https://doi.org/10.1016/j.jqsrt.2021.107949>
- 571 31. Vispoel B, Cavalcanti JH, Paige ET, Gamache RR. Vibrational dependence, temperature  
572 dependence, and prediction of line shape parameters for the  $\text{H}_2\text{O}-\text{N}_2$  collision system. *J Quant*  
573 *Spectrosc Radiat Transf* 2020;253:107030. <https://doi.org/10.1016/j.jqsrt.2020.107030>
- 574 32. Koroleva AO, Odintsova TA, Tretyakov M.Yu, Pirali O, Campargue A, The foreign-  
575 continuum absorption of water vapour in the far-infrared (50–500  $\text{cm}^{-1}$ ), *J. Quant. Spectrosc.*  
576 *Rad. Transf.* 261 (2021), 107486.